5714 *Biochemistry* **2010,** *49,* 5714–5725
DOI: 10.1021/bi100314n

BIOCHEMISTRY
including biophysical chemistry & molecular biology
Article

Disrupted Zinc-Binding Sites in Structures of Pathogenic SOD1 Variants D124V and H80R[†]

Sai V. Seetharaman,[‡,§] Duane D. Winkler,[‡,§] Alexander B. Taylor,[‡,§] Xiaohang Cao,[‡,§] Lisa J. Whitson,[‡,§] Peter A. Doucette,[∥] Joan S. Valentine,[∥] Virgil Schirf,[‡] Borries Demeler,[‡] Mark C. Carroll,[⊥] Valeria C. Culotta,[⊥] and P. John Hart*[,‡,§,@]

[‡]*Department of Biochemistry, and* [§]*X-ray Crystallography Core Laboratory, The University of Texas Health Science Center, San Antonio, Texas 78229,* [∥]*Department of Chemistry and Biochemistry, The University of California, Los Angeles, California 90095,* [⊥]*Department of Environmental Health Sciences, Johns Hopkins University Bloomberg School of Public Health, Baltimore, Maryland 21205, and* [@]*Geriatric Research, Education, and Clinical Center, Department of Veterans Affairs, South Texas Veterans Health Care System, San Antonio, Texas 78229*

Received March 2, 2010; Revised Manuscript Received May 28, 2010

ABSTRACT: Mutations in human copper−zinc superoxide dismutase (SOD1) cause an inherited form of the fatal neurodegenerative disease amyotrophic lateral sclerosis (ALS). Here, we present structures of the pathogenic SOD1 variants D124V and H80R, both of which demonstrate compromised zinc-binding sites. The disruption of the zinc-binding sites in H80R SOD1 leads to conformational changes in loop elements, permitting non-native SOD1−SOD1 interactions that mediate the assembly of these proteins into higher-order filamentous arrays. Analytical ultracentrifugation sedimentation velocity experiments indicate that these SOD1 variants are more prone to monomerization than the wild-type enzyme. Although D124V and H80R SOD1 proteins appear to have fully functional copper-binding sites, inductively coupled plasma mass spectrometery (ICP-MS) and anomalous scattering X-ray diffraction analyses reveal that zinc (not copper) occupies the copper-binding sites in these variants. The absence of copper in these proteins, together with the results of covalent thiol modification experiments in yeast strains with and without the gene encoding the copper chaperone for SOD1 (CCS), suggests that CCS may not fully act on newly translated forms of these polypeptides. Overall, these findings lend support to the hypothesis that immature mutant SOD1 species contribute to toxicity in SOD1-linked ALS.

Copper−zinc superoxide dismutase (SOD1)[1] detoxifies superoxide anion, a byproduct of cellular respiration, to molecular oxygen and hydrogen peroxide [$2O_2^- + 2H^+ \rightarrow H_2O_2 + O_2$] (*1*). In the early 1990s, mutations in the human gene encoding SOD1 were linked to the fatal, progressive neurodegenerative disease amyotrophic lateral sclerosis (ALS, Lou Gehrig's disease) (*2*, *3*). Today, more than 100 distinct pathogenic mutations have been documented (reviewed in refs (*4*) and (*5*)), with most resulting in single amino acid substitutions and a few in truncations of the polypeptide.

Seminal studies in transgenic mice have established that pathogenic SOD1 proteins give rise to motor neuron dysfunction through the gain of a toxic property and not a loss of enzymatic function. Mice expressing human fALS SOD1 polypeptides in addition to their endogenous active SOD1 develop paralytic symptoms (*6*−*8*), while SOD1 knockout mice do not (*9*). The appearance of inclusions enriched in mutant SOD1 in cell culture model systems, in ALS-SOD1 transgenic mice, and in fALS patients has led to the suggestion that SOD1-linked ALS toxicity is related to misfolding and/or aggregation of these polypeptides (reviewed in refs (*10*−*12*)). However, the precise molecular mechanisms underlying mutant SOD1 toxicity remain unknown, and it is unclear whether the observed proteinaceous inclusions cause or arise from motor neuron dysfunction.

The appearance of insoluble, higher-order assemblies of pathogenic SOD1 proteins in patients and in murine models of the disease strongly suggests that these SOD1 variants possess properties distinct from those of the wild-type enzyme that lead to their aggregation in vivo. Previous studies of wild-type SOD1 have highlighted the stabilizing roles of both metal ion binding and the presence of an oxidized intrasubunit disulfide bond (*13*−*15*). Both of these stabilizing posttranslational modifications of nascent SOD1 are facilitated by a helper protein called the copper chaperone for SOD1 (CCS) (*16*−*18*). Pathogenic SOD1 mutations that alter CCS/SOD1 protein−protein interactions or prevent proper CCS action could result in destabilized, immature SOD1 proteins that are prone to non-native self-association (*4*, *5*, *19*).

Here, we characterize the human pathogenic SOD1 variants D124V and H80R using single-crystal X-ray diffraction, analytical

[†]This work was supported by National Institutes of Health Grants NS39112 (P.J.H.), RR022200 (B.D.), NS049134 (J.S.V.), and GM50016 (V.C.C.), National Science Foundation Grant TG-MCB070038 (B.D.), and the Johns Hopkins University NIEHS center (V.C.C.). D.D.W. and L.J.W. were supported in part by an American Foundation for Aging Research predoctoral fellowship. X.C. and S.V.S. were supported in part by the Judith and Jean Pape Adams Charitable Foundation and the William and Ella Owens Medical Research Foundation.

*To whom correspondence should be addressed. E-mail: pjhart@biochem.uthscsa.edu. Telephone: (210) 567-0751. Fax: (210) 567-6595.

[1]Abbreviations: SOD1, copper−zinc superoxide dismutase; ALS, amyotrophic lateral sclerosis; fALS, familial amyotrophic lateral sclerosis; D124V, copper−zinc superoxide dismutase with D124 substituted with Val; H80R, copper−zinc superoxide dismutase with H80 substituted with Arg; CCS, copper chaperone for SOD1; 2DSA, two-dimensional spectrum analysis; SOMO, SOlution MOdeler; ASTFEM-RA, Adaptive Space-Time Finite Element Solution for Multicomponent-Reacting Systems; ICP-MS, inductively coupled plasma mass spectrometry; AMS, 4-acetamido-4′-maleimidylstilbene-2,2′-disulfonic acid; EDTA, ethylenediaminetetraacetic acid; PDB, Protein Data Bank; rmsd, root-mean-square deviation.

 Published on Web 06/01/2010

ultracentrifugation, and covalent thiol modification. The findings (1) reinforce previous observations that the absence of metal ions in the zinc-binding sites of SOD1 variants can result in nonnative intermolecular interactions that give rise to higher-order filamentous arrays (*20*), (2) reveal that both the D124V and H80R SOD1 homodimers are more prone to dissociation than the wild-type enzyme, and (3) suggest that unlike the wild-type enzyme, CCS may not be able to interact productively with these pathogenic SOD1 variants in vivo. The resulting metal-deficient, destabilized mutant SOD1 proteins can essentially be considered as trapped folding intermediates that may be prone to oligomerization in motor neurons.

EXPERIMENTAL PROCEDURES

Materials. Monobasic and dibasic potassium phosphate, yeast extract, peptone, dextrose (glucose), EDTA, sodium chloride, acetic acid, and sodium acetate (used for demetalation) were obtained from Fischer Scientific. Ammonium sulfate was purchased from US Biological. Tris base [tris(hydroxymethyl)aminoethane] was purchased from Research Products International. Sodium malonate was from Fluka. AMS (4-acetamido-4′-maleimidylstilbene-2,2′-disulfonic acid) was purchased from Invitrogen. Agarose, glycerol (ethylene glycol), and the protease inhibitor cocktail were obtained from Sigma. *Pfu* DNA polymerase and deoxyribonucleotides were purchased from Stratagene. Glass beads were obtained from Biospec. Crystallization screening kits were obtained from Qiagen, and crystal growth trays were purchased from Hampton Research. Phenyl Sepharose, DEAE Sephadex, and Sephadex G-75 resin beads were purchased from Pharmacia. All solutions unless otherwise noted in the text were prepared using deionized water passed through a Millipore ultra purification system.

Protein Expression and Purification. The human D124V and H80R SOD1 proteins used in this study were expressed, purified, stripped of metals (for analytical ultracentrifugation), and characterized by inductively coupled plasma mass spectrometry (ICP-MS) and electrospray ionization mass spectrometry as described previously (*14*).

Crystallization, Data Collection, Structure Determination, and Refinement. All crystals were grown at room temperature using the hanging drop vapor diffusion method. Protein concentrations for the D124V and H80R SOD1 samples used in crystallization trials were 8.0 and 18.7 mg/mL, respectively. Because D124V SOD1 tends to precipitate from solution over time, it could not be stored for later use and was therefore used in crystallization experiments immediately after purification and concentration. These SOD1 variants in 2.25 mM potassium phosphate (pH 7.0) and 160 mM sodium chloride were mixed with an equal volume of reservoir solution containing 2.4 M sodium malonate (pH 7.0) for D124V or 2.3 M ammonium sulfate and 100 mM Tris (pH 8.0) for H80R. Teardrop-shaped crystals of D124V SOD1 grew in space group $P2_12_12_1$ within one week. Slender, rodlike crystals of H80R SOD1 grew in space group $P2_1$, also within one week, while blocklike prisms of H80R SOD1 grew in space group $P2_12_12_1$ after approximately two months in the same crystallization drop as the monoclinic form. Specimens of each crystal form suitable for single-crystal X-ray diffraction work were soaked in a cryoprotectant consisting of reservoir solution made 15% (v/v) in ethylene glycol before being flash-cooled by being plunged into liquid nitrogen. Native diffraction data from the D124V and H80R orthorhombic crystal forms were collected at resolutions of 1.55 and 1.65 Å, respectively, at Advanced Light Source (Berkeley, CA) beamline 8.2.2 on an Area Detector Systems Corp. Q315R CCD detector. Native diffraction data from the monoclinic H80R crystal form were collected at a resolution of 1.85 Å at the X-ray Crystallography Core Laboratory at The University of Texas Health Science Center on a Rigaku FR-D High Flux X-ray generator equipped with Osmic purple optics and a Rigaku HTC imaging plate detector. All diffraction data were processed using the HKL2000 suite (*21*).

The identities of metal ions bound in the D124V and H80R SOD1 proteins "as purified" were determined by ICP-MS and by collection of diffraction data from D124V and H80R crystals using X-rays of wavelengths (energies) tuned to the copper and zinc absorption edges as described previously for the pathogenic SOD1 variant G85R (*22*). The scattering of X-rays is altered by a metal ion at its absorption edge (anomalous scattering), and this property causes the metal to be illuminated in an electron density map, revealing both its location and an estimate of the amount (occupancy) bound at each site. The energy of X-rays tuned to the copper edge illuminates zinc only very weakly, providing a means of discriminating between the two metal ions. Anomalous diffraction data from the D124V and H80R orthorhombic crystal forms were collected at beamline 8.2.1 at the Advanced Light Source on an Area Detector Systems Corp. Q315R CCD detector. The first data sets were collected at the zinc absorption edge and above the copper absorption edge, giving anomalous diffraction data: copper $f'' = 3.4$ e, and zinc $f'' = 3.9$ e. The second data sets were collected at a wavelength of 1.38 Å, at the copper and below the zinc absorption edges, giving anomalous data: copper $f'' = 3.9$ e, and zinc $f'' = 0.6$ e. The wavelengths for optimal copper and zinc anomalous diffraction at the Advanced Light Source were determined by monitoring the X-ray fluorescence of the crystals at an angle normal to the incident X-ray beam immediately prior to data collection.

The D124V and H80R SOD1 structures were determined by molecular replacement with MOLREP (*23*) using the structure of the human SOD1 variant G37R (Protein Data Bank entry 1AZV) (*24*) as the search model. Once positioned, the models were subjected to alternating cycles of refinement in PHENIX (*25*) followed by manual adjustment into σ_A-weighted electron density maps (*26*) with COOT (*27*). No stereochemical restraints were applied to the metal−ligand distances or bond angles during refinement.

Analytical Ultracentrifugation. All analytical ultracentrifugation experiments were performed with a Beckman Optima XL-I centrifuge in the Center for Analytical Ultracentrifugation of Macromolecular Assemblies at The University of Texas Health Science Center. Sedimentation velocity data were analyzed with ULTRASCAN (*28*) version 9.9 (*29*). All calculations were performed on the Lonestar cluster at the Texas Advanced Computing Center at The University of Texas (Austin, TX) and on the Jacinto cluster at the Bioinformatics Core Facility at The University of Texas Health Science Center. Velocity measurements were taken at 230 nm in a buffer containing 2.25 mM sodium phosphate (pH 7.0) and 160 mM NaCl. The samples were centrifuged at 20.4 °C and 60000 rpm, using standard Epon two-channel centerpieces. Hydrodynamic corrections for buffer density, viscosity, and partial specific volume were applied according to methods outlined by Laue (*30*) as implemented in ULTRASCAN (*28*). The partial specific volume was determined to be 0.725 cm^3/g for wild-type human SOD1 and for H80R SOD1, whereas the value for D124V SOD1 was 0.727 cm^3/g. All data were first analyzed by two-dimensional spectrum analysis

Table 1: X-ray Diffraction Data and Refinement Statistics[a]

	D124V, $P2_12_12_1$, 3H2P	H80R, $P2_12_12_1$, 3H2R	H80R, $P2_1$, 3H2Q	D124V, $P2_12_12_1$		H80R, $P2_12_12_1$	
				copper edge	zinc edge	copper edge	zinc edge
Data Collection							
cell dimensions							
a, *b*, *c* (Å)	39.92, 57.97, 105.02	40.25, 58.43, 104.83	35.24, 136.80, 56.36				
α, *β*, *γ* (deg)	90, 90, 90	90, 90, 90	90, 104.58, 90				
resolution (Å)	50.0−1.55 (1.61−1.55)	50.0−1.65 (1.71−1.65)	30.0−1.85 (1.92−1.85)	1.80 (1.86−1.80)	1.80 (1.86−1.80)	1.65 (1.71−1.65)	1.65 (1.71−1.65)
λ (Å)	1.0000	1.2820	1.5418	1.3781	1.2826	1.3786	1.2820
R_{sym} (on *I*) (%)	6.7 (56.6)	6.4 (38.5)	9.0 (53.1)	9.0 (52.5)	9.0 (48.6)	6.3 (41.4)	6.4 (38.5)
$I/\sigma I$	18.7 (2.3)	23.2 (5.5)	21.1 (3.4)	17.5 (6.2)	17.1 (6.7)	23.1(3.2)	23.2 (5.5)
completeness (%)	99.1 (96.0)	99.9 (99.5)	94.5 (95.3)	99.8 (100)	99.9 (99.9)	99.2 (93.7)	99.9 (99.5)
redundancy	5.9 (5.1)	7.2 (6.3)	6.8 (6.5)	6.7 (6.0)	6.6 (6.1)	6.7 (3.5)	7.2 (6.3)
Refinement							
resolution (Å)	50.0−1.55	50.0−1.65	30.0−1.85				
no. of reflections	35624	56897	41462				
R_{work}/R_{free} (%)	15.28/19.96	14.33/18.42	18.24/22.33				
no. of dimers per asymmetric unit	1	1	2				
no. of atoms							
protein	1856	1804	3772				
metal ion	3 (Zn)	2 (Zn)	4 (Zn)				
water	259	188	370				
ligand	14 (malonate)	10 (sulfate)	25 (sulfate)				
rmsd							
bond lengths (Å)	0.004	0.004	0.006				
bond angles (deg)	0.900	0.850	1.033				

[a]Values in parentheses are values for the highest-resolution bin.

(2DSA) (*31*) with simultaneous removal of time-invariant noise, and then by genetic algorithm refinement (*32*), followed by Monte Carlo analysis (*33*).

Sedimentation velocity data for freshly isolated D124V SOD1 preparations were also fit to a nonlinear model for a reversible monomer−dimer equilibrium using the Adaptive Space-Time Finite Element Solution for Multicomponent-Reacting Systems (ASTFEM-RA) (*34*) to obtain equilibrium constants and kinetic rate constants. Extinction coefficients at 280 nm for SOD1 were determined by the method of Gill and von Hippel (*35*) to be 6170 OD mol^{-1} cm^{-1}. Absorption profiles from multiple concentrations ranging between 220 and 340 nm were fit with ULTRASCAN (*28*) to a sum of five Gaussian functions. The extinction fit was calibrated at 280 nm with the extinction coefficient determined above to derive an extinction coefficient at 230 nm of 58596.1 OD mol^{-1} cm^{-1}. Bead models were calculated with ULTRASCAN SOlution MOdeler (SOMO) (*36*) which is available for free download from http://www.ultrascan.uthscsa.edu.

Covalent Modification of Free Thiols in SOD1. 4-Acetamido-4′-maleimidylstilbene-2,2′-disulfonic acid (AMS) was used to covalently modify free thiols in D124V and H80R SOD1 proteins coming from yeast with and without the *ccs1* gene as previously described (*37*) to monitor the degree to which the SOD1 intrasubunit disulfide bond is oxidized in these variants.

Figure Preparation. All figures were created using PyMOL (*58*).

RESULTS

Structures of D124V and H80R SOD1. The crystal structures of the pathogenic D124V and H80R SOD1 proteins were determined and refined at resolutions ranging from 1.55 to 1.85 Å. X-ray diffraction data collection and protein structure refinement statistics are listed in Table 1. Figure 1 reveals that while the Greek key *β*-barrels of D124V and H80R SOD1 remain similar in structure to that of the wild-type enzyme, the D124V and H80R substitutions give rise to substantial disorder in loops IV (the "zinc loop", residues 50−83) and VII (the "electrostatic loop", residues 121−142). Figure 2A shows that the electrostatic loop elements in adjacent metal-deficient H80R SOD1 dimers in the monoclinic crystal form can engage in reciprocal, non-native SOD1−SOD1 interactions at edge strands in the Greek key *β*-barrel that become accessible due to the inability of this variant to bind metal in the zinc-binding site. As shown in Figure 2B, these non-native SOD1−SOD1 contacts occur at opposite ends of the H80R SOD1 homodimer, permitting them to propagate bidirectionally over the entire length of the crystal to form higher-order filamentous arrays.

Disrupted Zinc-Binding Sites. Figure 3 shows that the D124V and H80R pathogenic SOD1 substitutions disrupt the zinc-binding sites in these variants. The degree of disorder of the zinc-binding sites is quite similar overall in all three structures, with an absence of electron density for H71 and only very poor electron density for H80 in each case.

Zinc in the Copper-Binding Sites. ICP-MS analyses performed on freshly purified D124V and H80R SOD1 variants prior to use in crystallization or analytical ultracentrifugation experiments indicated that although these proteins were completely devoid of copper, they contained between 1.5 and 1.7 equiv of zinc per dimer. Measurement of the fluorescence of D124V and H80R SOD1 crystals as they were scanned with X-rays at

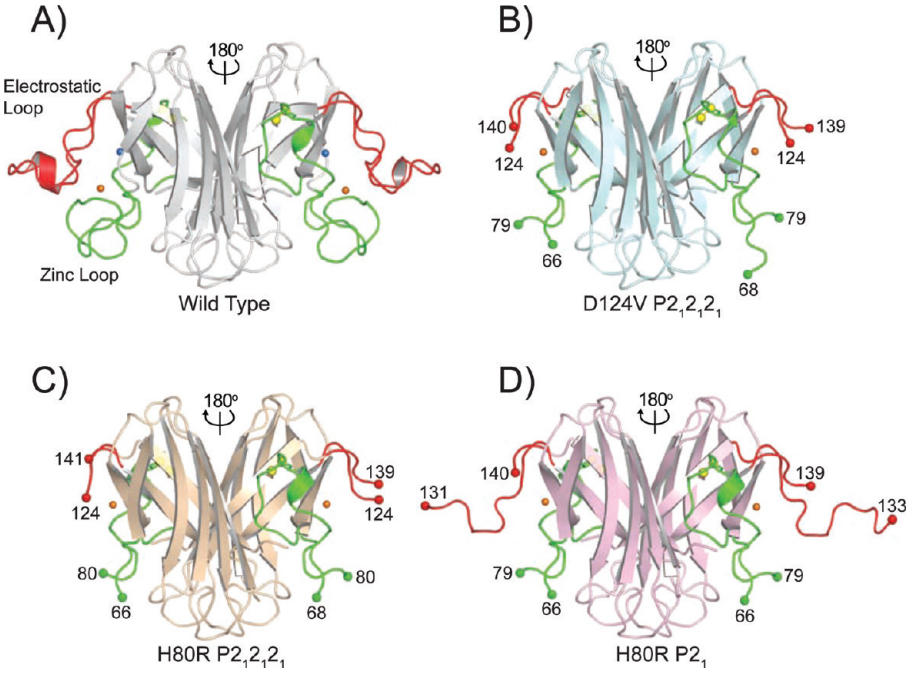

FIGURE 1: Structures of human wild-type, D124V, and H80R SOD1. (A) Human wild-type SOD1 [PDB entry 2c9v (*39*)]. The relationship between the two subunits in the SOD1 dimer is indicated. The Greek key β-barrel is colored gray, the zinc loop (loop IV, residues 50−83) green, and the electrostatic loop (loop VII, residues 121−142) red. Copper, zinc, and the sulfur atoms of C57 and C146 that form the disulfide bond in each subunit are shown as blue, orange, and yellow spheres, respectively. (B) Human D124V SOD1 variant in the same orientation as the wild-type enzyme shown in panel A. The color coding is the same as in panel A except the Greek key β-barrel is colored cyan. Green and red spheres represent the last residues visible in the electron density for the zinc and electrostatic loop elements, respectively. Zinc occupies the copper-binding site, and there is no metal in the zinc-binding site. (C) Human H80R SOD1 variant in space group $P2_12_12_1$. The color coding is the same as for the wild-type enzyme except the Greek key β-barrel is colored gold. Zinc occupies the copper-binding site, and there is no metal in the zinc-binding site. (D) Human H80R SOD1 variant in space group $P2_1$. The color coding is the same as for the wild-type enzyme except the Greek key β-barrel is colored pink. Zinc occupies the copper-binding site, and there is no metal in the zinc-binding site.

energies spanning the zinc and copper absorption edges, followed by inspection of anomalous difference Fourier electron density maps, confirmed the presence of zinc and the absence of copper in these pathogenic SOD1 variants. Supplementary Figure 1 (Supporting Information) reveals sharp transitions in the fluorescence spectra measured for D124V and H80R SOD1 crystals when the energy of the X-rays illuminating the crystals reaches the zinc absorption edge. In contrast, no sharp transitions are evident when the energy of the X-rays illuminating the crystals coincides with the copper absorption edge. Supplementary Figure 2 (Supporting Information) shows zinc and copper edge anomalous difference Fourier electron density maps superimposed on the refined D124V SOD1 structure. The zinc edge anomalous difference electron density peaks are very strong, persisting at contour levels greater than 60σ, while the anomalous difference Fourier electron density peaks coming from the small contribution of zinc at the copper edge ($f'' = 0.6$ e) disappear between 12σ and 13σ. As a comparison, the anomalous difference Fourier electron density peaks coming from the sulfur atoms of the four cysteine residues in each SOD1 subunit are no longer visible at contour levels greater than approximately 10σ. Nearly identical results were obtained using anomalous difference Fourier electron density maps obtained from the H80R SOD1 orthorhombic crystal form.

As shown in Figure 3, the zinc ions occupying the copper-binding sites in the D124V and H80R SOD1 variants are coordinated by H46, H48, and H120, at distances of ~2.0 Å. Depending upon which was present in the crystallization mother liquor, the oxygen atoms of malonate or sulfate anions act as a fourth ligand to the zinc (not shown in Figure 3 for the sake of clarity). The zinc coordination geometry in the D124V and H80R SOD1 proteins is best described as distorted tetrahedral, with the zinc ion displaced ~0.4 Å from the plane formed by the nitrogen atoms of the three liganding histidine ligands. This coordination geometry is quite similar to that observed for zinc in the copper-binding site in the 1.4 Å resolution structure of the pathogenic D125H SOD1 variant, which was crystallized in the presence of sulfate anion (*38*).

Oxidation of Cys111. Figure 4 shows σ_A-weighted electron density with coefficients $2mF_o - DF_c$ superimposed on the C111 residues in the H80R $P2_12_12_1$ crystal structure. The C111 Sγ atoms appear to be oxidized to sulfonic acid (Cys111-SO_3H) in subunit A and to sulfenic acid (Cys111-SOH) in subunit B.

Covalent Thiol Modification. Cysteine residues are found in human SOD1 at positions 6, 57, 111, and 146. C57 and C146 participate in the intrasubunit disulfide bond in the mature wild-type enzyme. To probe whether CCS can affect the redox status of this intrasubunit disulfide bond in the D124V and H80R SOD1 variants in cells, covalent thiol modification experiments were performed on these proteins after expression in *ccs1*+ and *ccs1*Δ yeast as previously described (*19*, *37*). Figure 5 reveals that when AMS is added to fresh lysates of *ccs1*Δ yeast expressing wild-type, D124V, or H80R SOD1, in each case, a fraction is observed to possess four free thiols that are covalently modified by AMS. When expressed in *ccs1*+ yeast, this fraction of wild-type SOD1 is converted to a species with only two free thiols, suggesting that CCS facilitates the oxidation of the C57−C146 disulfide bond. In contrast, the four thiol fractions of the D124V and H80R SOD1 proteins remain unaltered when these proteins are expressed in *ccs1*+ yeast, suggesting that CCS is unable to interact productively with these particular SOD1 variants.

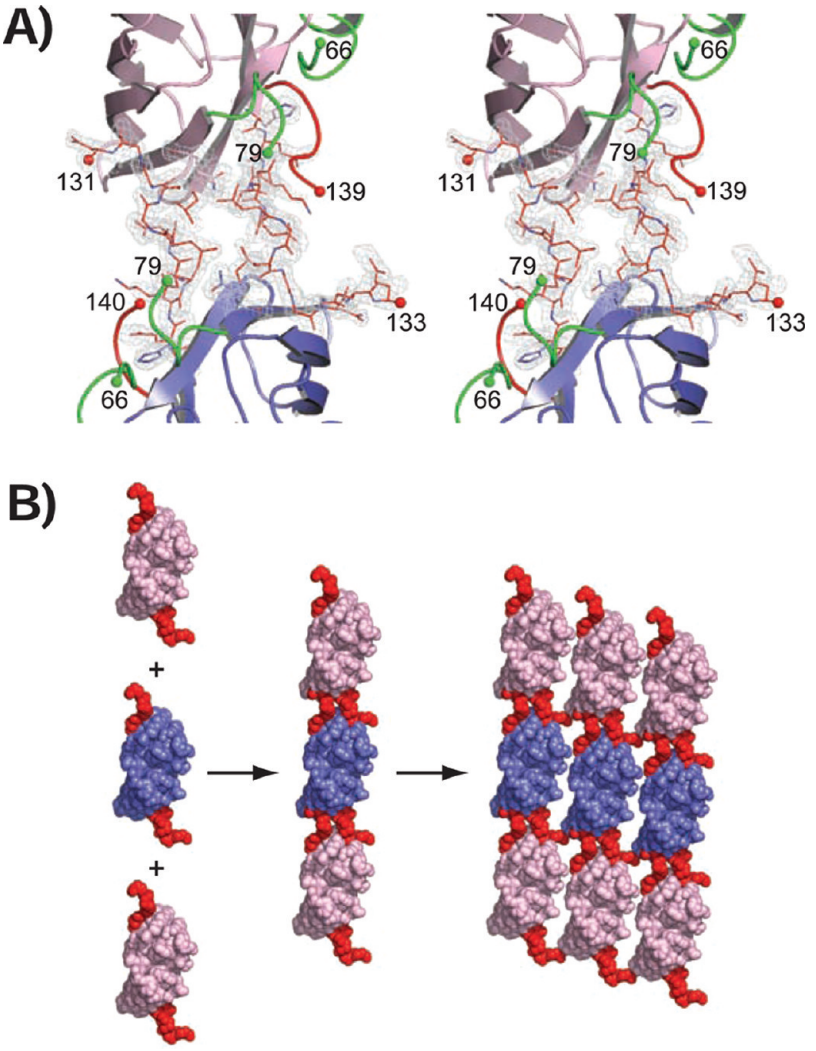

FIGURE 2: Divergent stereoview of the non-native contacts formed between adjacent H80R SOD1 homodimers in the $P2_1$ crystal form. Residues of the zinc and electrostatic loop elements are colored green and red, respectively. The Greek key β-barrel of a subunit coming from one SOD1 homodimer is colored pink, and that of another subunit coming from an adjacent SOD1 homodimer is colored blue. Green and red spheres represent the last residues visible in the electron density in the zinc and electrostatic loops, respectively. Residues 121−131 of the electrostatic loop from one H80R dimer interact with a depression in the β-barrel of a neighboring H80R dimer in the crystal lattice. The σ_A-weighted electron density, with coefficients $2mF_o - DF_c$, is contoured at 1.5σ. (B) Space-filling representation of H80R SOD1 proteins assembling into higher-order filamentous arrays in the $P2_1$ crystal form. The color coding is the same as in panel A except the zinc loop has not been colored green to more easily visualize the reciprocal interactions mediated by the electrostatic loop and β-barrel elements of adjacent H80R SOD1 dimers in the crystal lattice.

Analytical Ultracentrifugation. A comparison of the sedimentation coefficient distributions of D124V and H80R SOD1 with wild-type SOD1 is shown in Figure 6A. Plots of boundary fraction versus $s_{20,w}$ will be vertical if the sample is homogeneous and will have a positive slope if the sample is heterogeneous. Although the wild-type SOD1 protein sediments as a single, homogeneous species with an S value of 3.03, the D124V and H80R SOD1 proteins form a distribution of species ranging from ~1.7 to 2.6 S, consistent with a reversible monomer−dimer equilibrium (*14*). After metal ion removal, the D124V and H80R SOD1 variants exhibit a heterogeneous distribution ranging from 0.5 to 3.0 S. The D124V sample, when examined in the analytical ultracentrifuge after being stored at 4 °C for 10 days, displays a distribution identical to the distribution observed for the metal-free sample, suggesting that it loses its bound metal over time.

To further characterize the mass and shape distributions of these samples, the sedimentation velocity data were analyzed using whole boundary fitting to the Adaptive Space-Time Finite Element Solution for Multi-Component Reacting Systems (*34*). Consistent with the results of the analysis described above, wild-type SOD1 sediments as a single species with a sedimentation coefficient of 3.03 S, a frictional ratio of 1.21, and a molecular mass of 31.0 kDa, the latter of which is in excellent agreement with the theoretically determined molecular mass of the homodimer (31.95 kDa) (Figure 6A,C). The sedimentation velocity results for wild-type SOD1 were also compared to the hydrodynamic parameters derived from bead modeling of the X-ray crystal structure [PDB entry 2C9V (*39*)] using UltraScan SOMO (*36*). SOMO predicted the sedimentation coefficient for the wild type to be 3.06 S for the homodimer and the frictional ratio to be 1.22, in excellent agreement with the values obtained from the sedimentation velocity experiments.

The monomer−dimer fit of the sedimentation data for freshly isolated D124V SOD1 is shown in Figure 6B. The monomer−dimer equilibrium model parameters are listed in Table 2. The D124V SOD1 variant dissociates to monomers with an equilibrium constant of approximately 650 nM. The kinetics of this

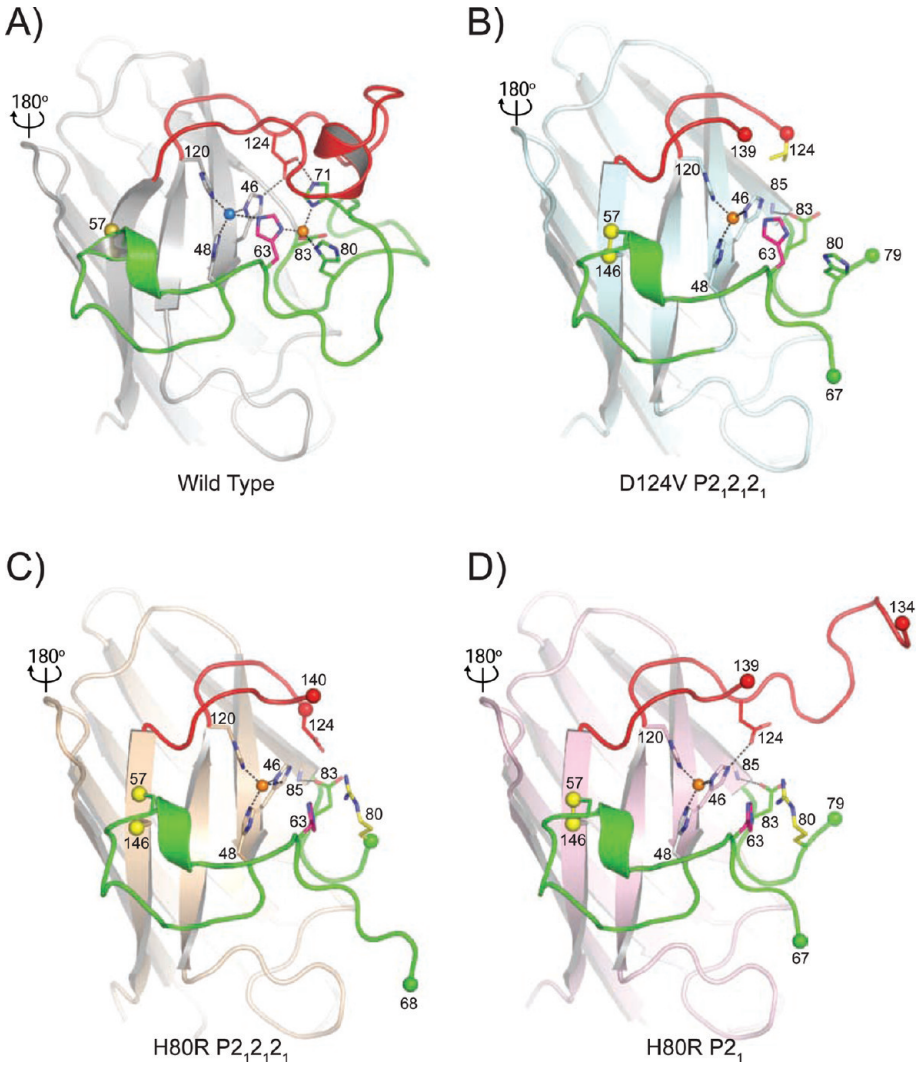

FIGURE 3: Metal-binding sites in human wild-type, D124V, and H80R SOD1. The color coding of the zinc and electrostatic loop elements is the same as in Figure 1. (A) Human wild-type SOD1 [PDB entry 2c9v (*39*)]. Metal−ligand bonds and hydrogen bonds between D124 and the nonliganding imidazole nitrogen atoms of copper ligand H46 and H71 are shown as dotted lines. H63, the bridging imidazolate, is colored magenta. (B) Human D124V SOD1 variant in the same orientation as the wild-type enzyme shown in panel A. Zinc occupies the copper-binding site, and there is no metal in the zinc-binding site. H63 is colored magenta and the D124V mutation yellow. Metal−ligand bonds and the hydrogen bond between D83 and N85 are shown as dotted lines. (C) Human H80R SOD1 variant in space group $P2_12_12_1$. Zinc occupies the copper-binding site, and there is no metal in the zinc-binding site. H63 is colored magenta and the H80R mutation yellow. Metal−ligand bonds and the hydrogen bond between D83 and N85 are shown as dotted lines. (D) Human H80R SOD1 variant in space group $P2_1$. Zinc occupies the copper-binding site, and there is no metal in the zinc-binding site. H63 is colored magenta and the H80R mutation yellow. Metal−ligand bonds and the hydrogen bonds between D83 and N85 and between D124 and H46 are shown as dotted lines.

dissociation are quite slow with a k_{off} rate of only 1.03×10^{-4} s^{-1}. A similar equilibrium constant of 660 nM is calculated when the data are fit to a noninteracting model (Table 2 and Figure 6C, top panel).

The sedimentation velocity data for freshly isolated H80R SOD1 were also fit to a monomer−dimer equilibrium model, which resulted in a binding constant of 143 nM (see Table 2). However, the genetic algorithm-Monte Carlo analysis reveals a species that does not correspond to a monomer−dimer molecular mass (see Figure 6C, bottom). While the dimer molecular mass is as expected (32.2 kDa), the second, much less abundant species appears to be globular with a molecular mass of 26.7 kDa. This result suggests that the second species may not be a reversible self-associating monomer but instead might be a degradation product. However, the concentration of the second species is too low to reliably determine its identity. In fact, in both the D124V and H80R metal-free SOD1 samples, several minor degradation products were detected whose concentration is too low to permit reliable identification. However, the increase in the frictional ratio for the dimeric forms of both pathogenic SOD1 mutants relative to the wild type strongly suggests that both the D124V and H80R mutants are more extended or unfolded than the wild-type enzyme, a suggestion consistent with the disordered regions of loops IV and VII shown in Figures 1 and 3.

DISCUSSION

The D124V and H80R Mutations Disrupt the Zinc-Binding Site. The crystal structures determined in this work suggest why the D124V and H80R pathogenic substitutions adversely affect the ability of these variants to bind zinc in the zinc-binding site. Figures 3A and 7A reveal that D124 is located in the electrostatic loop (loop VII, residues 121−142), where its side chain stabilizes both the copper- and zinc-binding sites by accepting hydrogen bonds simultaneously from the nonliganding imidazole nitrogen

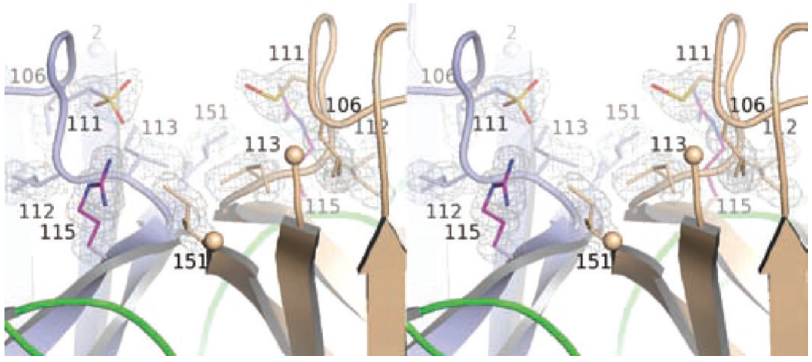

FIGURE 4: Divergent stereoview of the dimer interface in the H80R $P2_12_12_1$ structure showing the oxidation of C111 residues. Subunits A and B of the H80R homodimer are colored blue and gold, respectively. Residues of the zinc loop are colored green. The molecular model is superimposed on the σ_A-weighted electron density of the form $2mF_o - DF_c$ contoured at 1.5σ. The Sγ atom of C111 is oxidized to sulfonic acid in subunit A and sulfenic acid in subunit B. Except for R115, the environment immediately surrounding C111 is quite apolar. The proximity of R115 to C111 in this environment may lower the pK_a of C111, causing it to be "reactive" (see the text).

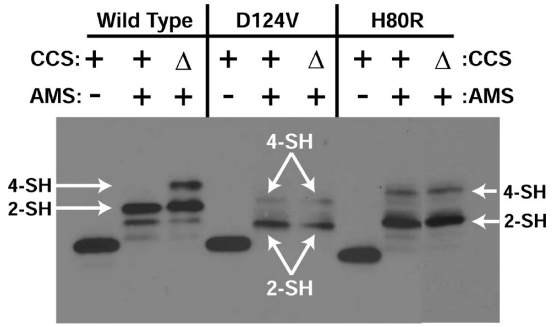

FIGURE 5: AMS covalent thiol modification of D124V and H80R SOD1 variants coming from *ccs1*Δ and *ccs1*+ yeast. The SOD1 monomer contains four cysteine residues, two of which participate in a conserved disulfide bond within each SOD1 subunit. *ccs1*Δ and *ccs1*+ yeast cells expressing D124V and H80R SOD1 are lysed in the presence of AMS, and the lysates are run on SDS−PAGE and probed with an antibody specific for SOD1 as described previously (*55*, *56*). AMS-modified thiols produce gel shifts to higher molecular weights such that two are modified in the disulfide-oxidized enzyme and four are modified in the disulfide-reduced enzyme. The disulfide status of the D124V and H80R SOD1 variants is predominantly oxidized and is unaffected by CCS.

atoms of copper ligand H46 and zinc ligand H71. These two D124-mediated hydrogen bonds are the primary interactions linking the electrostatic loop to the zinc loop, as well as anchoring these loop elements to the SOD1 β-barrel. The importance of the D124 side chain for proper metal binding to the zinc-binding site in SOD1 was noted previously when D124N and D124G SOD1 mutants were found to be severely zinc-deficient, even after extensive dialysis against 0.5 M $ZnCl_2$ at neutral pH (*40*). Figure 3B shows that the elimination of the hydrogen bonding interactions with H46 and H71 by the D124V substitution results in severely disordered electrostatic and zinc loop elements, the latter of which house the zinc ligands H63, H71, H80, and D83 (Table 3). Figure 7A shows that the side chain of zinc ligand D83 is oriented away from the zinc-binding site such that its $O_{\delta 1}$ atom, which coordinates the zinc ion in the wild-type enzyme, instead accepts a hydrogen bond from the amide nitrogen of G85.

Figures 3C,D and 7B show that the H80R pathogenic SOD1 substitution disrupts the zinc-binding site by sterically preventing zinc binding and by inducing conformational disorder in the electrostatic and zinc loop elements. Figure 7B shows that in addition to being a poor zinc ligand relative to histidine, the lengthy R80 side chain occupies the position held by the carbonyl oxygen of K136 in the wild-type enzyme, which prevents residues 132−136 of the electrostatic loop from forming the short α-helix that normally acts as a "lid" to shield the zinc-binding site from bulk solvent. As can be inferred from panels C and D of Figure 3, the R80-induced displacement of this helical lid permits the zinc loop to become conformationally dynamic, resulting in the displacement of the zinc ligand H71 such that it no longer resides within 15 Å of its original position in wild-type SOD1. The bridging imidazolate, H63, adopts a conformation such that it is unable to coordinate metal ions in either metal-binding site. Finally, as observed in the D124V structure, the zinc ligand, D83, adopts a conformation such that it points away from the position occupied by zinc in the wild-type enzyme.

Non-Native Higher-Order Assembly of H80R SOD1. Although the ability of metal-deficient, pathogenic SOD1 proteins to assemble into higher-order filamentous arrays was first described more than six years ago in structures of the pathogenic SOD1 variants S134N and H46R (*20*, *41*), the notion that the edges of β-strands 5 and 6 and the cleft between them may act as a "hot spot" for non-native pathogenic SOD1 self-association has recently gained momentum. For example, non-native intermolecular SOD1 interactions nearly identical to those shown in Figure 2A were observed in structures of wild-type human SOD1 proteins engineered to possess ablated zinc-binding sites (*42*, *43*). Recent work by Nordlund, Oliveberg, and colleagues is particularly notable because the non-native SOD1−SOD1 interactions highlighted in Figure 2A were also observed in the structure of an SOD1 protein engineered to be exclusively monomeric, which led them to suggest that the interactions at this interface may initiate aggregation of pathogenic SOD1 proteins in vivo (*42*, *43*). In each of these cases, the absence of metal ions in the zinc-binding site appears to be necessary for these non-native intermolecular SOD1 interactions to occur, consistent with the notion that immature SOD1 proteins may represent the noxious entities in SOD1-linked ALS (*4*, *5*, *19*).

C111 Oxidation. The electron density superimposed on C111 residues at the homodimeric interface in H80R SOD1 shown in Figure 4 strongly suggests that the sulfur atoms are oxidized to sulfonic acid (C111-SO_3H) in subunit A and to sulfenic acid (C111-SOH) in subunit B. Interestingly, these adducts are clearly observed on the H80R SOD1 variant in the $P2_12_12_1$ crystal form but not in the $P2_1$ crystal form, even though these crystals were grown from the same crystallization drop. A similar partitioning of SOD1 species upon crystallization was observed previously for

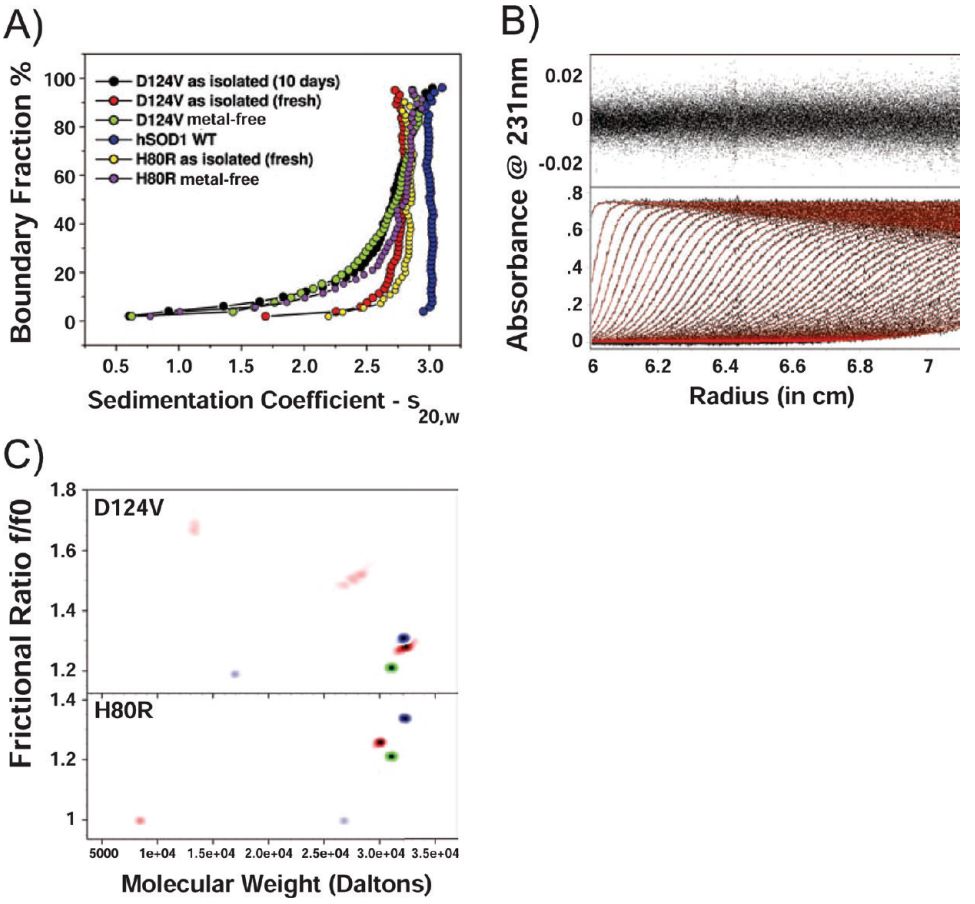

FIGURE 6: Analytical ultracentrifugation of wild-type, and D124V, and H80R SOD1. (A) van Holde and Weischet integral distribution plot of sedimentation coefficients for wild-type hSOD1 (blue) and D124V and H80R mutants. Data for freshly isolated D124V and H80R mutants are colored red and yellow, respectively, while data for their metal-free forms are colored green and purple, respectively. D124V is also shown after being stored for 10 days at 4 °C (black). After 10 days, the sedimentation coefficient distribution appears identical to that of the apo form, suggesting the loss of metal from the D124V SOD1 protein over time. Human wild-type SOD1 sediments as a homogeneous species with a sedimentation coefficient of 3.03 S, consistent with a homodimer. The D124V and H80R mutant SOD samples exhibited various degrees of heterogeneity. (B) D124V SOD1 sedimentation velocity data fitted with a reversible monomer−dimer model based on the ASTFEM-RA solution (*34*). The equilibrium constant, shape factors, and rate constants are listed in Table 2. The residuals of the fit are shown in the top panel and are randomly distributed, suggesting that the monomer−dimer model is a good representation of these data. The bottom panel shows the experimental sedimentation velocity data (black), and the ASTFEM-RA model overlay is colored red. (C) Results for the Monte Carlo fit of sedimentation velocity data from the metal-free form (red) and the freshly isolated sample (blue) of D124V (top) and H80R (bottom). Data for human wild-type SOD1 are colored green for comparison in both panels. Both mutants show an increase in the frictional ratio for the dimer relative to the wild-type enzyme.

G85R SOD1 and H46R/H48Q SOD1. G85R SOD1 was found to crystallize in four distinct crystal forms such that each crystal form contained a metal-bound species distinct from those in the other crystal forms (*22*), while H46R/H48Q SOD1 was observed to crystallize in two distinct crystal forms in which one displayed diatomic covalent adducts to C111 while the other did not (*19*).

Several reports have implicated C111 in human SOD1 as a "reactive" cysteine. In addition to the oxidation products described above and in ref *44*, there have been reports of covalent modification of C111 by glutathione (*45*) and by sulfur to form persulfide (*46*, *47*), trisulfide (*48*), and, more recently, a heptasulfane bridge linking the two SOD1 subunits at the homodimeric interface (*57*). We speculate that the reactive nature of C111 may arise from the nature of its local environment. Figure 4 shows that C111 is tucked into a recessed cavity located at the SOD1 dimer interface that is lined with apolar residues except for R115. The proximity of the positive charge coming from the R115 guanidinium moiety in an apolar environment that is partially protected from the solvent might lower the pK_a of the C111 thiol, enhancing its reactivity.

Dissociation of D124V and H80R SOD1 Dimers. As shown in Figure 6C, freshly purified D124V and H80R SOD1 dimers with zinc in the copper-binding site demonstrate greater f/f_0 ratios than the wild-type SOD1 homodimer, suggesting that the differences in $s_{20,w}$ between the ~2.6 S D124V and H80R SOD1 dimers and the ~3.0 S metal-bound wild-type SOD1 dimers shown in Figure 6A are due to differences in shape rather than mass. The observation of a greater frictional ratio for the D124V and H80R SOD1 variants is consistent with the observation of disordered zinc and electrostatic loop elements observed in their crystal structures as shown in Figure 3 because conformational disorder of these loop elements would be expected to enhance the drag of these molecules, thereby decreasing their S values relative to the wild-type dimer with its well-ordered zinc and electrostatic loops.

The binding of metal ions to SOD1 has long been known to have an enormous stabilizing effect on the SOD1 homodimer (reviewed in refs *14* and *49*). When metal-free, however, disulfide-oxidized human wild-type SOD1 proteins still do not fractionally dissociate into monomers under even the most dilute concentrations

Table 2: Results of Analytical Ultracentrifugation Analyses[a]

	reversible monomer−dimer self-association model	noninteracting model
	D124V	
monomer molecular mass	16.1 (15.8, 16.4) kDa	16.8 (16.6, 17.1) kDa
dimer molecular mass	constrained to 2 × monomer molecular mass	31.8 (31.6, 3.23) kDa (unconstrained)
monomer f/f_0	1.12 (1.09, 1.14)	1.19 (1.18, 1.20)
dimer f/f_0	1.29 (1.28, 1.31)	1.31 (1.30, 1.31)
$K_{dissociation}$	0.65 (0.49, 0.96) μM	0.66 μM (based on partial concentrations)
k_{off} rate constant	1.03×10^{-4} (0.96×10^{-4}, 1.11×10^{-4}) s^{-1}	not available
k_{on} rate constant	6.69×10^{-5} M s^{-1}	not available
	H80R	
monomer molecular mass	16.9 (16.8, 17.0) kDa	29.1 (26.9, 29.7) kDa[b]
dimer molecular mass	constrained to 2 × monomer molecular mass	30.6 (30.1, 32.8) kDa (unconstrained)
monomer f/f_0	[b]	1.0 (1.0, 1.0)
dimer f/f_0	1.32 (1.31, 1.32)	1.27 (1.25, 1.36)
$K_{dissociation}$	0.143 (0.142, 0.144) μM	[b]
k_{off} rate constant	[b]	not available
k_{on} rate constant	[b]	not available

[a]Fitting parameters for the freshly isolated mutant D124V and H80R SOD1 samples. Values in parentheses represent 95% confidence intervals determined in the Monte Carlo analysis. Both the reversible self-association model and the noninteracting model give very similar results and are fitted equally well to the data. [b]The second species determined in this fit did not correspond to the monomer molecular mass, and therefore, the equilibrium constant cannot be calculated.

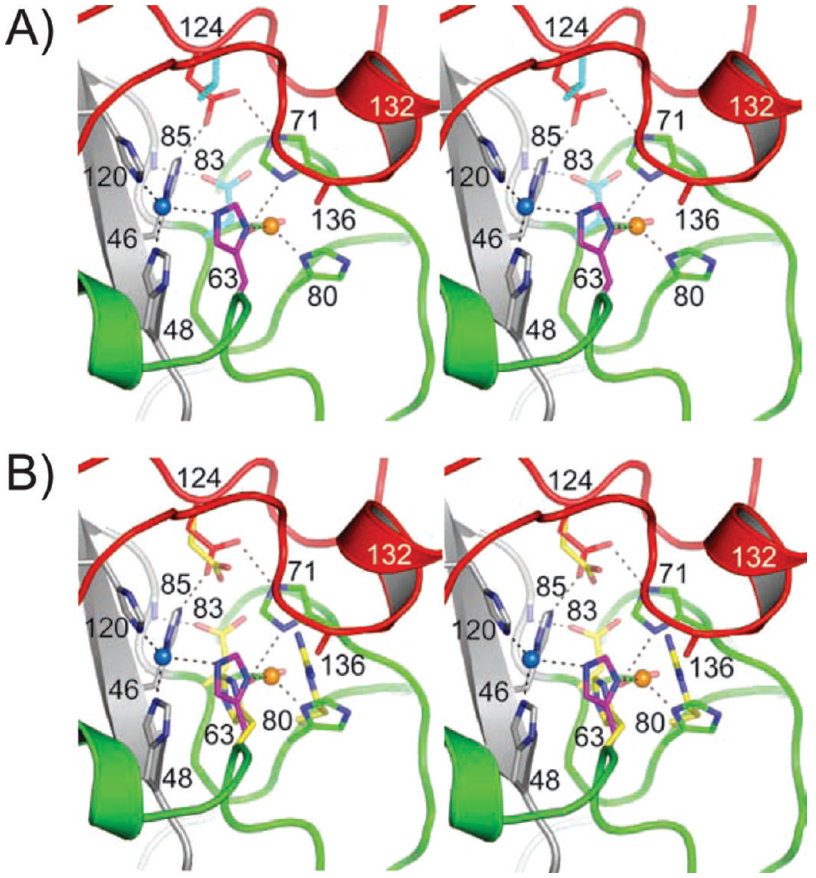

FIGURE 7: Metal-binding site of human wild-type SOD1 on the D124V and H80R SOD1 variants. The color coding of the zinc and electrostatic loop elements is as in Figure 1. (A) D124V SOD1 superimposed on human wild-type SOD1 [PDB entry 2c9v (*39*)]. Only the side chains of residues 83 and 124 are shown coming from the D124V structure. (B) H80R SOD1 superimposed on human wild-type SOD1 [PDB entry 2c9v (*39*)]. Only the side chains of residues 63, 80, 83, and 124 are shown coming from the H80R structure. The R80 side chain clashes with the carbonyl oxygen of K136, disrupting the α-helix formed by residues 132−136 of the H80R electrostatic loop (see the text).

used in sedimentation equilibrium experiments (2 μM) (*14*), which is indicative of a dimerization K_d of ≤10 nM. In contrast, despite the fact that the D124V and H80R SOD1 proteins possess an oxidized disulfide bond (Figure 5) and bind metal ions in their copper-binding sites (Figure 3), they remain significantly weaker dimers than metal-free, disulfide-oxidized wild-type SOD1 as indicated by the positive slopes of their van Holde and Weischet plots shown in Figure 6A, as well as their calculated dissociation

Table 3: Disordered Regions and Identities of Metal Ions in the Metal-Binding Sites

					metal-binding sites	
monomer	disordered regions	primary bridge (H63)	secondary bridge (D124)	D83 orientation	copper site (occupancy)	zinc site (occupancy)
			D124V, $P2_12_12_1$			
A	67−78 125−139	broken	broken	flipped	zinc (0.8)	zinc (0.15)
B	69−77 125−138	broken	broken	flipped	zinc (0.9)	empty
			H80R, $P2_12_12_1$			
A	67−78 131−138	broken	intact	wild type	zinc (0.7)	empty
B	69−78 125−138	broken	intact	flipped	zinc (0.9)	empty
			H80R, $P2_1$			
A	67−78 134−138	broken	intact	flipped	zinc (0.7)	empty
B	67−78 133−139	intact	intact	flipped	zinc (0.6)	empty
C	67−79 125−140	intact	intact	flipped	zinc (0.2)	empty
D	67−78 126−138	broken	intact	flipped	zinc (0.7)	empty

constants of 650 and 143 nM, respectively (Table 2). A potential implication of these differences in the dissociation behavior of D124V and H80R SOD1 proteins relative to that of the wild type with regard to CCS action is explored more fully below.

Hindered CCS-Mediated Maturation and SOD1-Linked ALS. When expressed in *sod1*Δ/*ccs1*+ yeast, wild-type SOD1 proteins rescue the oxygen sensitive phenotype of these yeast and contain substantial amounts of both copper and zinc when purified (*24*, *50*, *51*). In contrast, H46R, D124V, and H80R SOD1 proteins expressed in these yeast are unable to rescue the oxygen-sensitive phenotype, an observation that is consistent with ICP-MS and anomalous scattering analyses indicating that these SOD1 variants are completely devoid of copper (*20*). The results of the covalent thiol modification experiments shown in Figure 5 suggest that CCS has no apparent effect on the disulfide bond status of the D124V and H80R variants. Taken together, these observations might be indicative of an inability of CCS to interact with newly translated D124V and H80R variants in a productive fashion.

In contrast to the D124V and H80R SOD1 proteins studied here, crystal structures of human H46R/H48Q SOD1 reveal zinc bound to the zinc-binding sites and ablated copper-binding sites (*19*). H46R/H48Q SOD1 proteins were observed to form stable heterocomplexes with CCS under reducing conditions in native gel electrophoresis experiments, but in AMS covalent thiol modification experiments analogous to those conducted in this study, H46R/H48Q SOD1 remained disulfide-reduced, even when expressed in *ccs1*+ yeast (*19*). Thus, in the case of the H46R/H48Q SOD1 variant, interaction with CCS is not sufficient for CCS to catalyze the oxidation of the intrasubunit disulfide bond. Because copper delivery and disulfide bond oxidation of SOD1 proteins by CCS are postulated to be coupled processes, the inability of H46R/H48Q SOD1 to accept copper from CCS might also prevent CCS-mediated oxidation of its disulfide bond (*16*, *18*, *52*).

The fact that CCS fails to activate D124V and H80R SOD1 proteins with copper, even though these variants possess what appear to be normal copper-binding sites, is somewhat puzzling. As mentioned above, one possibility might be that interactions between CCS and these variants is weakened, a notion supported by the observation of an enhanced propensity of D124V and H80R SOD1 proteins to dissociate relative to the wild-type enzyme. The weakened affinity of D124V and H80R SOD1 subunits for themselves in the homodimer might also translate into a weakened affinity for SOD1-like domain 2 of CCS that is responsible for the specificity of CCS−SOD1 interactions. Although this seems like a plausible suggestion, additional experiments are necessary to test this hypothesis.

We and others have demonstrated that the affinity of CCS for disulfide-oxidized forms of SOD1 is substantially lower than for disulfide-reduced forms (*18*, *19*, *53*, *54*), and the data in Figure 5 reveal that the D124V and H80R SOD1 proteins are predominantly disulfide-oxidized whether CCS is present in yeast cells expressing these variants. This observation is intriguing in itself because if CCS cannot productively engage D124V and H80R SOD1, the fraction of disulfide-reduced D124V and H80R proteins in these experiments might be expected to be at least as large as that observed for the wild-type enzyme or for the H46R/H48Q variant. A possible explanation for these somewhat puzzling observations might be that oxidation of the SOD1 intrasubunit disulfide bond in yeast may depend more on whether a metal is bound at the copper-binding site than on the identity of the metal ion per se, as long as oxygen and/or superoxide are present. In this context, the reduced disulfide bond observed in H46R/H48Q SOD1 in previous AMS thiol modification experiments (*19*) might arise from the inability of this variant to bind any metal ion at its copper-binding site, while the predominantly oxidized disulfide bond observed in the D124V and H80R SOD1 variants could arise from the fact that they can bind a metal (zinc) in their respective copper-binding sites. In summary, the results presented here for the structural and biophysical properties of the D124V and H80R pathogenic SOD1 variants, together with previous observations on the H46R/H48Q SOD1 variant, are

consistent with the suggestion that incomplete posttranslational modification of nascent SOD1 polypeptides may be a characteristic associated with toxicity in SOD1-linked ALS.

ACKNOWLEDGMENT

We acknowledge the support provided by the staff at the Texas Advanced Computing Center at The University of Texas and by Jeremy Mann at the Bioinformatics Core Facility at The University of Texas Health Science Center. Support for the X-ray Crystallography Core Laboratory and the Center for Analytical Ultracentrifugation of Macromolecular Assemblies by The University of Texas Health Science Center Executive Research Committee and the San Antonio Cancer Institute is also gratefully acknowledged

SUPPORTING INFORMATION AVAILABLE

Fluorescence of D124V and H80R SOD1 crystals measured normal to the X-ray beam at energies spanning the zinc and copper edges (Supplementary Figure 1) and anomalous difference Fourier electron density calculated at various contour levels with diffraction data taken from orthorhombic D124V SOD1 crystals with X-rays tuned to the zinc and copper absorption edges superimposed on the refined D124V SOD1 structure (Supplementary Figure 2). This material is available free of charge via the Internet at http://pubs.acs.org.

REFERENCES

1. Fridovich, I. (1989) Superoxide dismutases. An adaptation to a paramagnetic gas. *J. Biol. Chem. 264*, 7761–7764.
2. Deng, H. X., Hentati, A., Tainer, J. A., Iqbal, Z., Cayabyab, A., Hung, W. Y., Getzoff, E. D., Hu, P., Herzfeldt, B., Roos, R. P., Warner, C., Deng, G., Soriano, E., Smyth, C., Parge, H. E., Ahmed, A., Roses, A. D., Hallewell, R. A., Pericak-Vance, M. A., and Siddique, T. (1993) Amyotrophic lateral sclerosis and structural defects in Cu,Zn superoxide dismutase. *Science 261*, 1047–1051.
3. Rosen, D. R., Siddique, T., Patterson, D., Figlewicz, D. A., Sapp, P., Hentati, A., Donaldson, D., Goto, J., O'Regan, J. P., Deng, H. X., Rahmani, Z., Krizus, A., McKenna-Yasek, D., Cayabyab, A., Gaston, S. M., Berger, R., Tanzi, R. E., Halperin, J. J., Herzfeldt, B., Van den Bergh, R., Hung, W.-Y., Bird, T., Deng, G., Mulder, D. W., Smyth, C., Laing, N. G., Soriano, E., Pericak-Vance, M. A., Haines, J., Rouleau, G. A., Gusella, J. S., Horvitz, H. R., and Brown, R. H., Jr. (1993) Mutations in Cu/Zn superoxide dismutase gene are associated with familial amyotrophic lateral sclerosis. *Nature 362*, 59–62.
4. Winkler, D. D., Prudencio, M., Karch, C. M., Borchelt, D. R., and Hart, P. J. (2009) Copper-Zinc Superoxide Dismutase, its Copper Chaperone, and Familial Amyotrophic Lateral Sclerosis. In Protein Misfolding Diseases: Current and Emerging Principles and Therapies (Dobson, C. M., Kelly, J. W., and Ramirez-Alvarado, M., Eds.) John Wiley & Sons, Inc., Hoboken, NJ.
5. Seetharaman, S. V., Prudencio, M., Karch, C., Holloway, S. P., Borchelt, D. R., and Hart, P. J. (2009) Immature Copper-Zinc Superoxide Dismutase and Familial Amyotrophic Lateral Sclerosis. *Exp. Biol. Med. 234*, 1140–1154.
6. Bruijn, L. I., Becher, M. W., Lee, M. K., Anderson, K. L., Jenkins, N. A., Copeland, N. G., Sisodia, S. S., Rothstein, J. D., Borchelt, D. R., Price, D. L., and Cleveland, D. W. (1997) ALS-linked SOD1 mutant G85R mediates damage to astrocytes and promotes rapidly progressive disease with SOD1-containing inclusions. *Neuron 18*, 327–338.
7. Gurney, M. E., Pu, H., Chiu, A. Y., Dal Canto, M. C., Polchow, C. Y., Alexander, D. D., Caliendo, J., Hentati, A., Kwon, Y. W., and Deng, H. X.; et al. (1994) Motor neuron degeneration in mice that express a human Cu,Zn superoxide dismutase mutation. *Science 264*, 1772–1775.
8. Wang, J., Xu, G., Li, H., Gonzales, V., Fromholt, D., Karch, C., Copeland, N. G., Jenkins, N. A., and Borchelt, D. R. (2005) Somatodendritic accumulation of misfolded SOD1-L126Z in motor neurons mediates degeneration: αB-Crystallin modulates aggregation. *Hum. Mol. Genet. 14*, 2335–2347.
9. Reaume, A. G., Elliott, J. L., Hoffman, E. K., Kowall, N. W., Ferrante, R. J., Siwek, D. F., Wilcox, H. M., Flood, D. G., Beal, M. F., Brown, R. H., Jr., Scott, R. W., and Snider, W. D. (1996) Motor neurons in Cu/Zn superoxide dismutase-deficient mice develop normally but exhibit enhanced cell death after axonal injury. *Nat. Genet. 13*, 43–47.
10. Bruijn, L. I., Miller, T. M., and Cleveland, D. W. (2004) Unraveling the mechanisms involved in motor neuron degeneration in ALS. *Annu. Rev. Neurosci. 27*, 723–749.
11. Hart, P. J. (2006) Pathogenic superoxide dismutase structure, folding, aggregation and turnover. *Curr. Opin. Chem. Biol. 10*, 131–138.
12. Valentine, J. S., Doucette, P. A., and Zittin Potter, S. (2005) Copper-zinc superoxide dismutase and amyotrophic lateral sclerosis. *Annu. Rev. Biochem. 74*, 563–593.
13. Arnesano, F., Banci, L., Bertini, I., Martinelli, M., Furukawa, Y., and O'Halloran, T. V. (2004) The unusually stable quaternary structure of human Cu,Zn-superoxide dismutase 1 is controlled by both metal occupancy and disulfide status. *J. Biol. Chem. 279*, 47998–48003.
14. Doucette, P. A., Whitson, L. J., Cao, X., Schirf, V., Demeler, B., Valentine, J. S., Hansen, J. C., and Hart, P. J. (2004) Dissociation of human copper-zinc superoxide dismutase dimers using chaotrope and reductant. Insights into the molecular basis for dimer stability. *J. Biol. Chem. 279*, 54558–54566.
15. Lindberg, M. J., Normark, J., Holmgren, A., and Oliveberg, M. (2004) Folding of human superoxide dismutase: Disulfide reduction prevents dimerization and produces marginally stable monomers. *Proc. Natl. Acad. Sci. U.S.A. 101*, 15893–15898.
16. Brown, N. M., Torres, A. S., Doan, P. E., and O'Halloran, T. V. (2004) Oxygen and the copper chaperone CCS regulate posttranslational activation of Cu,Zn superoxide dismutase. *Proc. Natl. Acad. Sci. U.S.A. 101*, 5518–5523.
17. Culotta, V. C., Klomp, L. W., Strain, J., Casareno, R. L., Krems, B., and Gitlin, J. D. (1997) The copper chaperone for superoxide dismutase. *J. Biol. Chem. 272*, 23469–23472.
18. Furukawa, Y., and O'Halloran, T. V. (2006) Posttranslational modifications in Cu,Zn-superoxide dismutase and mutations associated with amyotrophic lateral sclerosis. *Antioxid. Redox Signaling 8*, 847–867.
19. Winkler, D., Schuermann, J., Cao, X., Holloway, S., Borchelt, D., Carroll, M., Proescher, J., Culotta, V., and Hart, P. (2009) Structural and Biophysical Properties of the Pathogenic SOD1 Variant H46R/H48Q. *Biochemistry. 48*, 3436–3447.
20. Elam, J. S., Taylor, A. B., Strange, R., Antonyuk, S., Doucette, P. A., Rodriguez, J. A., Hasnain, S. S., Hayward, L. J., Valentine, J. S., Yeates, T. O., and Hart, P. J. (2003) Amyloid-like filaments and water-filled nanotubes formed by SOD1 mutant proteins linked to familial ALS. *Nat. Struct. Biol. 10*, 461–467.
21. Otwinowski, Z., and Minor, W. (1997) Processing of X-ray diffraction data collected in oscillation mode. In Methods in Enzymology (Carter, C. W., and Sweet, R. M., Eds.) pp 307−326, Academic Press, New York.
22. Cao, X., Antonyuk, S. V., Seetharaman, S. V., Whitson, L. J., Taylor, A. B., Holloway, S. P., Strange, R. W., Doucette, P. A., Valentine, J. S., Tiwari, A., Hayward, L. J., Padua, S., Cohlberg, J. A., Hasnain, S. S., and Hart, P. J. (2008) Structures of the G85R variant of SOD1 in familial amyotrophic lateral sclerosis. *J. Biol. Chem. 283*, 16169–16177.
23. Vagin, A. A., and Teplyakov, A. (1997) MOLREP: An automated program for molecular replacement. *J. Appl. Crystallogr. 30*, 1022–1025.
24. Hart, P. J., Liu, H., Pellegrini, M., Nersissian, A. M., Gralla, E. B., Valentine, J. S., and Eisenberg, D. (1998) Subunit asymmetry in the three-dimensional structure of a human CuZnSOD mutant found in familial amyotrophic lateral sclerosis. *Protein Sci. 7*, 545–555.
25. Adams, P. D., Grosse-Kunstleve, R. W., Hung, L. W., Ioerger, T. R., McCoy, A. J., Moriarty, N. W., Read, R. J., Sacchettini, J. C., Sauter, N. K., and Terwilliger, T. C. (2002) PHENIX: Building new software for automated crystallographic structure determination. *Acta Crystallogr. D58*, 1948–1954.
26. Read, R. J. (1986) *Acta Crystallogr. A42*, 140–149.
27. Emsley, P., and Cowtan, K. (2004) Coot: Model-building tools for molecular graphics. *Acta Crystallogr. D60*, 2126–2132.
28. Demeler, B. (2005) UltraScan: A Comprehensive Data Analysis Software Package for Analytical Ultracentrifugation Experiments. In Modern Analytical Ultracentrifugation: Techniques and Methods (Scott, D., Harding, S., and Rowe, A., Eds.) pp 210−229, Royal Society of Chemistry, Cambridge, U.K.
29. Demeler, B. (2009) UltraScan: An comprehensive data analysis software package for analytical ultracentrifugation experiments. http://www.ultrascan.uthscsa.edu/.
30. Laue, T. M., Shah, B. D., Ridgeway, T. M., and Pelletier, S. L. (1992) Computer-aided interpretation of analytical sedmentation data for

proteins. In Analytical Ultracentrifugation in Biochemistry and Polymer Science (Harding, S. E., Rowe, A. J., and Horton, J. C., Eds.) pp 90−125, Royal Society of Chemistry, Cambridge, U.K.
31. Brookes, E., Cao, W., and Demeler, B. (2009) A two-dimensional spectrum analysis for sedimentation velocity experiments of mixtures with heterogeneity in molecular weight and shape. *Eur. Biophys. J. 39*, 405–414.
32. Brookes, E., and Demeler, B. (2007) Parsimonious Regularization using Genetic Algorithms Applied to the Analysis of Analytical Ultracentrifugation Experiments. GECCO Proceedings ACM 978-1-59593-697-4/07/0007.
33. Demeler, B., and Brookes, E. (2008) Monte Carlo analysis of sedimentation experiments. *Colloid Polym. Sci. 286*, 129–137.
34. Cao, W., and Demeler, B. (2008) Modeling analytical ultracentrifugation experiments with an adaptive space-time finite element solution for multicomponent reacting systems. *Biophys. J. 95*, 54–65.
35. Gill, S. C., and von Hippel, P. H. (1989) Calculation of protein extinction coefficients from amino acid sequence data. *Anal. Biochem. 182*, 319–326.
36. Brookes, E., Demeler, B., Rosano, C., and Rocco, M. (2010) The implementation of SOMO (SOlution MOdeller) in the UltraScan analytical ultracentrifugation data analysis suite: Enhanced capabilities allow the reliable hydrodynamic modeling of virtually any kind of biomacromolecule. *Eur. Biophys. J. 39*, 423–435.
37. Carroll, M. C., Outten, C., Proescher, J. B., Rosenfeld, L., Watson, W. H., Whitson, L. J., Hart, P. J., Jensen, L. T., and Culotta, V. C. (2006) The effects of glutaredoxins and copper activation pathways on the disulfide and stability of Cu/Zn superoxide dismutase. *J. Biol. Chem. 281*, 28648–28656.
38. Elam, J. S., Malek, K., Rodriguez, J. A., Doucette, P. A., Taylor, A. B., Hayward, L. J., Cabelli, D. E., Valentine, J. S., and Hart, P. J. (2003) An alternative mechanism of bicarbonate-mediated peroxidation by copper-zinc superoxide dismutase: Rates enhanced via proposed enzyme-associated peroxycarbonate intermediate. *J. Biol. Chem. 278*, 21032–21039.
39. Strange, R. W., Antonyuk, S. V., Hough, M. A., Doucette, P. A., Valentine, J. S., and Hasnain, S. S. (2006) Variable metallation of human superoxide dismutase: Atomic resolution crystal structures of Cu-Zn, Zn-Zn and as-isolated wild-type enzymes. *J. Mol. Biol. 356*, 1152–1162.
40. Banci, L., Bertini, I., Cabelli, D. E., Hallewell, R. A., Tung, J. W., and Viezzoli, M. S. (1991) A characterization of copper/zinc superoxide dismutase mutants at position 124. Zinc-deficient proteins. *Eur. J. Biochem. 196*, 123–128.
41. Antonyuk, S., Elam, J. S., Hough, M. A., Strange, R. W., Doucette, P. A., Rodriguez, J. A., Hayward, L. J., Valentine, J. S., Hart, P. J., and Hasnain, S. S. (2005) Structural consequences of the familial amyotrophic lateral sclerosis SOD1 mutant His46Arg. *Protein Sci. 14*, 1201–1213.
42. Nordlund, A., Leinartaite, L., Saraboji, K., Aisenbrey, C., Grobner, G., Zetterstrom, P., Danielsson, J., Logan, D. T., and Oliveberg, M. (2009) Functional features cause misfolding of the ALS-provoking enzyme SOD1. *Proc. Natl. Acad. Sci. U.S.A. 106*, 9667–9672.
43. Roberts, B. R., Tainer, J. A., Getzoff, E. D., Malencik, D. A., Anderson, S. R., Bomben, V. C., Meyers, K. R., Karplus, P. A., and Beckman, J. S. (2007) Structural characterization of zinc-deficient human superoxide dismutase and implications for ALS. *J. Mol. Biol. 373*, 877–890.
44. Fujiwara, N., Nakano, M., Kato, S., Yoshihara, D., Ookawara, T., Eguchi, H., Taniguchi, N., and Suzuki, K. (2007) Oxidative modification to cysteine sulfonic acid of Cys111 in human copper-zinc superoxide dismutase. *J. Biol. Chem. 282*, 35933–35944.
45. Wilcox, K. C., Zhou, L., Jordon, J. K., Huang, Y., Yu, Y., Redler, R. L., Chen, X., Caplow, M., and Dokholyan, N. V. (2009) Modifications of Superoxide Dismutase (SOD1) in Human Erythrocytes: A Possible Role in Amyotrophic Lateral Sclerosis. *J. Biol. Chem. 284*, 13940–13947.
46. Calabrese, L., Federici, G., Bannister, W. H., Bannister, J. V., Rotilio, G., and Finazzi-Agro, A. (1975) Labile sulfur in human superoxide dismutase. *Eur. J. Biochem. 56*, 305–309.
47. de Beus, M. D., Chung, J., and Colon, W. (2004) Modification of cysteine 111 in Cu/Zn superoxide dismutase results in altered spectroscopic and biophysical properties. *Protein Sci. 13*, 1347–1355.
48. Okado-Matsumoto, A., Guan, Z., and Fridovich, I. (2006) Modification of cysteine 111 in human Cu,Zn-superoxide dismutase. *Free Radical Biol. Med. 41*, 1837–1846.
49. Bertini, I., Mangani, S., and Viezzoli, M. S. (1998) Structure and Properties of Copper-Zinc Superoxide Dismutase. *Adv. Inorg. Chem. 45*, 127–251.
50. Goto, J. J., Gralla, E. B., Valentine, J. S., and Cabelli, D. E. (1998) Reactions of hydrogen peroxide with familial amyotrophic lateral sclerosis mutant human copper-zinc superoxide dismutases studied by pulse radiolysis. *J. Biol. Chem. 273*, 30104–30109.
51. Goto, J. J., Zhu, H., Sanchez, R. J., Nersissian, A., Gralla, E. B., Valentine, J. S., and Cabelli, D. E. (2000) Loss of in vitro metal ion binding specificity in mutant copper-zinc superoxide dismutases associated with familial amyotrophic lateral sclerosis. *J. Biol. Chem. 275*, 1007–1014.
52. Furukawa, Y., Torres, A. S., and O'Halloran, T. V. (2004) Oxygen-induced maturation of SOD1: A key role for disulfide formation by the copper chaperone CCS. *EMBO J. 23*, 2872–2881.
53. Lamb, A. L., Torres, A. S., O'Halloran, T. V., and Rosenzweig, A. C. (2000) Heterodimer formation between superoxide dismutase and its copper chaperone. *Biochemistry 39*, 14720–14727.
54. Lamb, A. L., Torres, A. S., O'Halloran, T. V., and Rosenzweig, A. C. (2001) Heterodimeric structure of superoxide dismutase in complex with its metallochaperone. *Nat. Struct. Biol. 8*, 751–755.
55. Carroll, M. C., Outten, C. E., Proescher, J. B., Rosenfeld, L., Watson, W. H., Whitson, L. J., Hart, P. J., Jensen, L. T., and Cizewski Culotta, V. (2006) The effects of glutaredoxin and copper activation pathways on the disulfide and stability of Cu,Zn superoxide dismutase. *J. Biol. Chem. 281*, 28648–28656.
56. Proescher, J. B., Son, M., Elliott, J. L., and Culotta, V. C. (2008) Biological effects of CCS in the absence of SOD1 enzyme activation: Implications for disease in a mouse model for ALS. *Hum. Mol. Genet. 17*, 1728–1737.
57. You, Z., Cao, X., Taylor, A. B., Hart, P. J., and Levine, R. L. (2010) Characterization of a covalent polysulfane bridge in copper-zinc superoxide dismutase. *Biochemistry 49*, 1191–1198.
58. DeLano, W. L. (2002) The PyMOL Molecular Graphics System, DeLano Scientific, San Carlos, CA.